Structural and magnetic properties of $La_{1-x}Pr_xMnO_{3+\delta}$ ($0 \leqslant x \leqslant 1.0$)

V. Dyakonov,[1,2,*] F. Bukhanko,[2] V. Kamenev,[2] E. Zubov,[2] S. Baran,[3] T. Jaworska-Gołąb,[3] A. Szytuła,[3] E. Wawrzyńska,[3] B. Penc,[3] R. Duraj,[4] N. Stüsser,[5] M. Arciszewska,[1] W. Dobrowolski,[1] K. Dyakonov,[6] J. Pientosa,[1] O. Manus,[1] A. Nabialek,[1] P. Aleshkevych,[1] R. Puzniak,[1] A. Wisniewski,[1] R. Zuberek,[1] and H. Szymczak[1]

[1]*Institute of Physics, Polish Academy of Sciences, Aleja Lotników 32/46, 02-668 Warsaw, Poland*

[2]*A. A. Galkin Donetsk Physico-Technical Institute NASU, 83114 Donetsk, Ukraine*

[3]*M. Smoluchowski Institute of Physics, Jagiellonian University, Reymonta 4, 30-059 Kraków, Poland*

[4]*Institute of Physics, Technical University of Krakow, Podchorążych 1, 30-084 Kraków, Poland*

[5]*BENSC, Hahn-Meitner Institute, Glienicker Strasse 100, D-14109 Berlin-Wannsee, Germany*

[6]*A. F. Ioffe Physico-Technical Institute, 192021 St.-Petersburg, Russia*

(Received 3 April 2006; revised manuscript received 25 May 2006; published 19 July 2006)

X-ray, neutron powder diffraction (NPD), and magnetic measurements were performed in order to investigate the effect of Pr substitution for La on crystallographic structure, on character of magnetic ordering, and on transition temperature in $La_{1-x}Pr_xMnO_{3+\delta}$ manganites series ($0 \leqslant x \leqslant 1.0$). Strong dependence of structural and magnetic properties on average *A*-site ionic radius was found. The magnetic phase diagram, characterizing Pr concentration dependence of the phase transition temperature, was constructed, based on magnetic and on NPD results. In the compounds with $x < 0.7$, the ferromagneticlike behavior with ferromagnetic moment aligned along the *b* axis was observed in the temperature interval below the Curie temperature, T_C, varying in the range of 113–153 K, down to Mn ions canted spin arrangement transition temperature, T_{CANT}, varying in the range of 73–115 K. It was found that T_C changes nonmonotonously with Pr content, it decreases rapidly for $x < 0.3$ and for $x > 0.6$, while is practically independent on x for $0.3 < x < 0.6$. The Mn magnetic moments increase from 3.2 for $x=0$ to 3.6 for $x=0.3$ before decreasing to 1.7 μ_B/Mn for $x=1.0$ and form a canting structure with canting angle decreasing from 32° for $x=0$ to 16° for $x=0.3$ and then increasing to 70° for $x=1.0$. The NPD and x-ray diffraction data indicate that Pr doping in $LaMnO_3$ is accompanied by changes of both the lattice parameters and crystal structure. The compound with $x=0$ was shown to have a rhombohedral crystal structure, while the samples with $0.1 \leqslant x \leqslant 0.6$ have orthorhombic symmetry with a small Jahn-Teller distortion (or pseudocubic) which continuously transforms towards highly distorted orthorhombic structure for $x > 0.6$. From ac magnetic susceptibility, studied under hydrostatic pressure up to 1.5 GPa, it was found that T_C and T_{CANT} change linearly with an applied pressure. The results are interpreted taking into account the competition of ferromagnetic double-exchange and antiferromagnetic superexchange interactions. This competition leads to a low temperature disordered system with spin canted features as a result of a decrease of the average *A*-site cation radius followed by decrease of Mn-O bond lengths, Mn-O-Mn bond angles, and the static Jahn-Teller distortion of the MnO_6 octahedra.

DOI: 10.1103/PhysRevB.74.024418 PACS number(s): 75.47.Lx, 75.30.Kz, 61.12.Ex, 61.10.Eq

I. INTRODUCTION

Structural and magnetic properties of manganites are sensitive both to the manganese valency and to internal (chemical) factors such as an average A-site cationic radius $\langle r_A \rangle$ and a size mismatch at the *A* site, represented by the cation-size disorder parameter $\sigma^2 = \Sigma_i y_i r^2_i - \langle r_i \rangle^2$, where y_i and r_i are the fractional occupancies and the ionic radii of the *i* cation, respectively.[1–8] The ionic radii of the *A*-site cation may influence dramatically the structural parameters, the electron bandwidth and, consequently, the magnetic interactions. In hole-doped manganites $La_{1-x}A_xMnO_3$ both a decrease of $\langle r_A \rangle$ and an increase of σ^2 are established to diminish the phase transition temperature.[1,2] Therefore, in order to understand deeper the magnetic phenomena in manganite oxides in the case of replacement of La by a smaller rare-earth ion, systematic studies of their physical properties over a wide range of compositions seem to be useful.

The $x=0$ and $x=1.0$ end members of the $La_{1-x}Pr_xMnO_3$ family are insulators and antiferromagnets. The pure $LaMnO_3$ compound has a distorted perovskite structure and is antiferromagnetic[9–11] below $T_N = 140$ K. In $LaMnO_3$ the ferromagnetically ordered *ab* planes are stacked antiferromagnetically along the *c* axis. The A_y-type antiferromagnetic ordering was established to occur in the pure $PrMnO_3$ compound with the manganese moments aligned in the [010] direction.[12] In these compounds, the cooperative Jahn-Teller effect reduces the total energy of the system lowering the symmetry of the oxygen octahedra that surround Mn^{3+} ($t^3_{2g}e^1_g$) ions. The distortion breaks a degeneracy of the e_g electronic configuration, and orbital ordering of Mn^{3+} ions occurs, which is responsible for antiferromagnetic (AFM) stacking of ferromagnetic planes.

Double-exchange (DE) interaction[13,14] between Mn^{3+} and Mn^{4+} ions, occurring usually due to a substitution of La sites by divalent Ca^{2+} or Sr^{2+} ions or due to creation of vacancies in the rare-earth, manganese, or oxygen sites in the $LaMnO_3$ compound, is responsible for ferromagnetic ordering in manganites. The competition between the ferromagnetic DE and AFM superexchange interactions can lead to different spin arrangements depending on the Mn^{3+}/Mn^{4+} ratio.

The influence of the Pr cation upon physical properties of $Pr_{1-x}(Ca,Sr)_xMnO_3$ compounds was intensively studied.[4–8,15–25] X-ray and neutron diffraction measurements have shown a variety of crystal and magnetic structures in $Pr_{1-x}Ca_xMnO_3$ $(0 \leqslant x \leqslant 1)$ system.[4,5,8,15] A decrease of the *A*-site cation radius stabilizes the static Jahn-Teller distortions and leads to a weakening of ferromagnetic coupling. The phase transition temperature is found to decrease linearly when Pr content increases. In the electron-doped $Pr_{0.1}Ca_{0.9}MnO_3$ compound, the canted AFM order was found, while the $Pr_{0.7}Ca_{0.3}MnO_3$ compound exhibits the magnetic behavior similar to that of a spin glass.[19,20] In $Pr_{0.3}Ca_{0.7}MnO_3$, besides ferromagnetic ordering of Mn moments ($T_C \approx 210$ K), an additional magnetic transition has been found at ≈50 K, which could result from the depinning of magnetic domain walls at certain temperature and magnetic field.[16] The $Pr_{0.5}Sr_{0.5}MnO_3$ manganite was shown to exhibit two magnetic transitions, namely, from a paramagnetic (PM) to ferromagnetic (FM) state and from a FM state to AFM.[23] For ABO_3-type manganites, the canted spin phase was found to be stabilized stronger for the *A*-site ion with smaller radius.[21] The low temperature state of $(La_{1-y}Pr_y)_{0.7}Ca_{0.3}MnO_3$ is canted AFM insulator for $y > 0.8$ and FM metal for $y < 0.6$. In the range $0.6 < y < 0.8$, the magnetic state is a mixture of canted FM and AFM regions.[24] A neutron powder diffraction study of a rare-earth deficient $Pr_{0.9}MnO_3$ has shown that Mn ions order with a canted spin arrangement. The temperatures of magnetic ordering of Mn and Pr ions are equal to $T_N \approx 86$ K and $T_C \approx 53$ K, respectively.[25]

The properties of $La_{1-x}Pr_xMnO_{3+\delta}$ are expected to be no less interesting than those of $Pr_{1-x}(Ca,Sr)_xMnO_3$. This special type of manganite is less well known than others, and its detailed investigation is worthwhile. The main motivation for studies performed was to obtain data on the internal pressure effect on an evolution of properties of doped manganites caused by the decreasing $\langle r_A \rangle$ at constant electronic doping, and in particular a comprehensive study of this system in the entire doping range $(x=0-1.0)$. This system was chosen for a systematical investigation because a trivalent Pr ion with a small ionic radius substitution for La^{3+} (the ionic radii for Pr^{3+} and La^{3+} are equal to 1.179 Å and 1.216 Å, respectively[26]) should change the exchange interactions between Mn ions through modifications of both the Mn-Mn distances and the Mn-O-Mn angles without hole doping by a divalent ion for La. As a result, the large effects related to lattice distortion and magnetic disorder might be expected to appear. A very important reason for this study was to establish the structural and magnetic phase diagrams and to understand the basic mechanisms determining the evolution of structural and magnetic properties as a function of $\langle r_A \rangle$.

We have examined a series of eleven samples in which the average ionic radius of the *A* site systematically varied, while the carrier concentration remained fixed. The x-ray and neutron powder diffraction (NPD), magnetization, and ac magnetic susceptibility including under pressure studies are reported. The application of a broad spectrum of complementary experimental methods has allowed us to receive complete information on the effect of Pr substitution for La on crystallographic structure, character of magnetic ordering, and on phase transition temperature for the whole series of $La_{1-x}Pr_xMnO_3$ $(x=0-1.0)$ manganites.

In the first section, we have focused on the structural changes induced by varying $\langle r_A \rangle$, an information on which has been obtained using the x-ray and NPD measurements. The results indicate that there are two structural phase transitions with increasing Pr content. An evolution of both the symmetry and crystal lattice parameters was presented. Three crystallographic phases were shown to exist in this phase diagram, namely, rhombohedral ($R\bar{3}c$) for $x=0$, orthorhombic with a small Jahn-Teller distortion for $0.1 \leqslant x \leqslant 0.6$, and orthorhombic (*Pnma*) for $x > 0.6$.

In the second section, using the magnetic data we present the internal pressure effect (i.e., structural distortions induced by change of $\langle r_A \rangle$) on magnetic properties and character of magnetic ordering. The phase transition temperature was shown to be very sensitive to internal pressure and to decrease nonmonotonously with increasing *x*. As $\langle r_A \rangle$ decreases, there is a gradual tendency towards reduction of magnetic moment and there is no evidence of magnetization saturation for Pr-rich samples up to 12 kOe. This phenomenon was interpreted as a gradual canting of the magnetic moments with increasing Pr content. The Mn ions ordering with a canted spin arrangement was found to occur in the entire doping range $(x=0-1.0)$ below the canted spin transition temperature, T_{CANT}. A shift of inverse susceptibility to lower temperatures with decreasing $\langle r_A \rangle$ indicates a decrease of the magnetic interaction between Mn moments. Based on the magnetic and NPD results, the magnetic phase diagram of $La_{1-x}Pr_xMnO_{3+\delta}$ characterizing the concentration dependence of the phase transition temperature was constructed. It contains three different magnetic phases, namely, paramagnetic phase (above the Curie temperature); ferromagnetic state of the F_y type for Pr content $x < 0.7$ in temperature interval from T_C down to the temperature T_{CANT} below which the magnetic transition to the state with a canted spin arrangement of C_xF_y type takes place.

At the end of the paper, the evolution of $La_{1-x}Pr_xMnO_{3+\delta}$ properties versus internal (chemical) factors, based on the measurement data, is discussed. The results obtained suggest that there is significant coupling between magnetism and the crystal lattice in this system. The magnetic properties have been examined within the framework of double-exchange. The origin of peculiarities of structural and magnetic behavior in $La_{1-x}Pr_xMnO_{3+\delta}$ was shown to be due to the competition between ferromagnetic and antiferromagnetic interactions. This competition gives rise to low temperature disordered system with spin canted features as a result of a decrease of the average *A*-site cation radius followed by a decrease of both Mn-O-Mn bond angle and the static Jahn-Teller distortion of the MnO_6 octahedra.

II. EXPERIMENT

For the present studies all the $La_{1-x}Pr_xMnO_{3+\delta}$ samples with *x* ranging from 0 to 1.0 were prepared in the same manner in order to avoid the influence of secondary effects

on studied properties. The samples were prepared using high-purity lanthanum, praseodymium, and manganese oxides taken in stoichiometric ratio. The mixture was dissolved in diluted (1:1) nitric acid. The obtained solution was evaporated to a complete removal of water followed by a degrading of nitrite salts at 500–700 °C. The product obtained was grinded and then heated to 900–950 °C to remove salt-disintegration products. The above processes give a homogeneous distribution of components. The produced powders were compacted into briquettes 15 mm in diameter and heat treated during three stages at temperatures of 1000, 1100, and 1150 °C for 15 h each with intermediate grinding of as-obtained products. In order to obtain the ceramic samples, the manganite powders were compacted under pressure of 1 GPa into pellets 6 mm in diameter and in 1.2 mm thickness. Then they were sintered in air at 1170 °C for 20 h followed by temperature decrease to the room temperature at the rate of 70°/h. The value of $\delta \approx 0.08$ for the prepared samples was determined by the gravimetric and iodine methods.

In order to determinate both phase purity and the crystallographic structure, all the samples were characterized at room temperature with the both polycrystalline Philips diffractometer (PW 3020) working in the Bragg-Brentano geometry and DRON-3 diffractometer using the CuK_α radiation. Analysis of x-ray diffraction data indicates that the samples obtained are single phase, homogeneous, with well-formed crystalline structure.

The neutron powder diffraction measurements have been carried out in the temperature range 1.5–290 K that allowed us to analyze both the crystallographic and magnetic structures and their evolution as a function of Pr concentration. The NPD patterns were collected using the E6 diffractometer installed at the BER II reactor (Hahn-Meitner Institut, Berlin). The incident neutron wavelength was 2.439 Å. The data were analyzed using the Rietveld-type refinement program FULLPROF.[27]

The zero-field-cooled (ZFC) and field-cooled (FC) magnetization measurements were carried out on pressed powder pellets of cylindrical shape ($d=3$ mm, $l=6$ mm) over a temperature range of 4.2–300 K using PAR model 4500 vibrating sample magnetometer. The ac susceptibility measurements were carried out in the temperature range of 4.2–200 K at frequencies of 48 Hz–10 kHz with Lake Shore 7229 ac susceptometer using a mutual inductance bridge with an excitation field $H_{ac}=5.0$ Oe. Magnetic susceptibility measurements under hydrostatic pressure up to 1.5 GPa were performed on homemade susceptometer over a temperature range of 55–180 K in low magnetic field with the maximum induction of 10 Oe and at frequency of several hundred Hz. The voltage induced in the pickup coils was measured by a selective lock-in-amplifier, and the pressure was generated by a Unipress compressor type IF-012. For these measurements, a pressure container of CuBe with inner diameter of 12 mm was used with gaseous helium as a pressure-transmitting medium. The pressure was determined by a manganin coil pressure sensor.

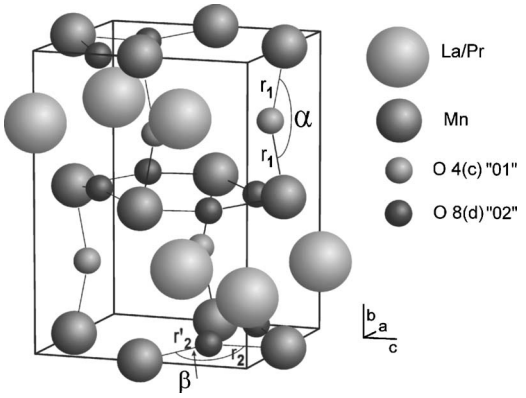

FIG. 1. Crystal structure of the manganite perovskite: r_1 (Mn-O1), r_2, [Mn-O2(1)], and r'_2 (Mn-O2) are the Mn-O bond lengths and α and β are the Mn-O-Mn bond angles.

III. RESULTS

A. Crystal structure

In the crystal structure of the manganite perovskite presented in Fig. 1, one can distinguish three Mn-O bond lengths (r_1, r_2, and r'_2) and the two Mn-O-Mn bond angles (α and β).

Both the symmetry and the values of crystal lattice parameters were derived from the positions and character of splitting of the perovskite pseudocubic lattice reflexes (Fig. 2).

It was found that the $LaMnO_{3+\delta}$ sample crystallizes in the rhombohedral structure (space group $R\,\bar{3}c$) with the following atomic positions: La atoms in the 2(a) site are 1/4, 1/4, 1/4; Mn atoms in the 2(b) site are 0, 0, 0; and O atoms in the 6(e) site are x, $1/2-x$, 1/4 with $x=0.808(3)$. The lattice parameter a_R is equal to 5.4788 Å and the angle α is equal to 60.7°. The lack of orthorhombic distortion of the unit cell characteristic for $LaMnO_3$ ($x=0$) indicates the formation of vacancies at La and Mn positions due to the presence of excess oxygen ($\delta \approx 0.08$), corresponding to the Mn^{4+} concentration $n=16\%$ ($\approx 100 \times 2\delta$).[28] The symmetry and the crystal lattice parameters change with increasing praseodymium content. The transition between rhombohedral unit cell and orthorhombic one (ORT-2) with a small Jahn-Teller distortion (or pseudocubic) takes place between $x=0$ and $x=0.1$. The latter continuously transforms towards highly distorted orthorhombic unit cell (ORT-1) above $x=0.6$. The existence of two orthorhombic (ORT-1 and ORT-2) crystallographic structures in manganites with La and Mn vacancies was reported in Ref. 29. In pseudocubic phase, the average value of the lattice constants is equal to $a \approx c \approx b/\sqrt{2} \approx 5.5$ Å. All of the Bragg reflections observed in the x-ray diffraction pattern for $x>0.6$ can be indexed in the orthorhombic crystallographic unit cell (space group *Pnma*) with the La/Pr and O1 atoms occupying the 4(c) site are x, 1/4, z; Mn atoms in the 4(b) site are 0, 0, 1/2; and O2 atoms in the 8(d) site are x, y, z. The lattice parameters and atomic positional parameters of O1 and O2 are collected in Table I. The dependence of both the lattice constants a, b, and c and the unit cell volume V on Pr content is shown in Fig. 3. The a, b,

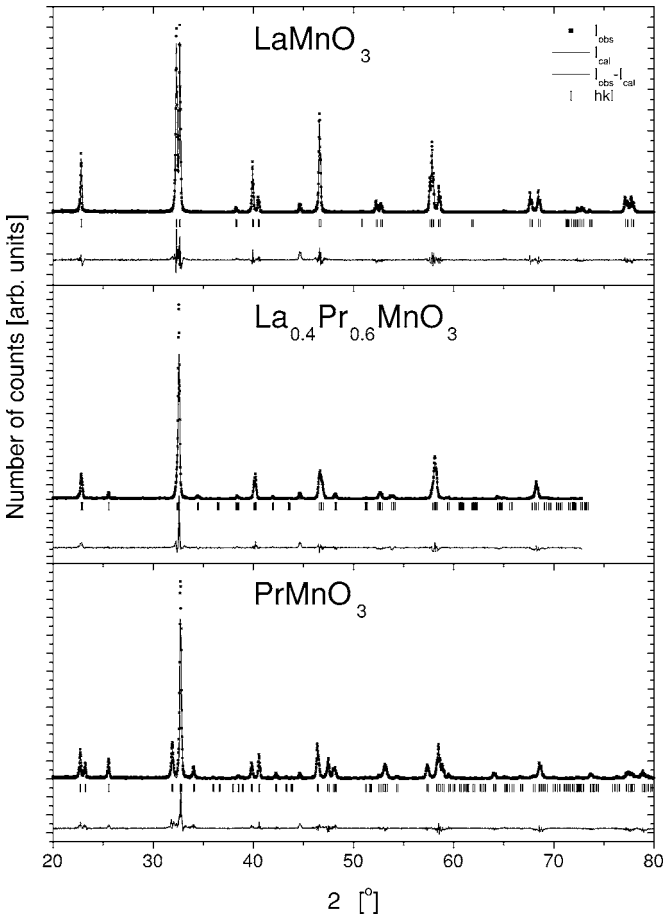

FIG. 2. Room temperature x-ray diffraction patterns of the $La_{1-x}Pr_xMnO_3$ manganites with $x=0$, 0.6, and 1.0, observed (solid squares) and calculated (solid lines). Bragg reflections are indicated by tick marks and the difference pattern is also plotted.

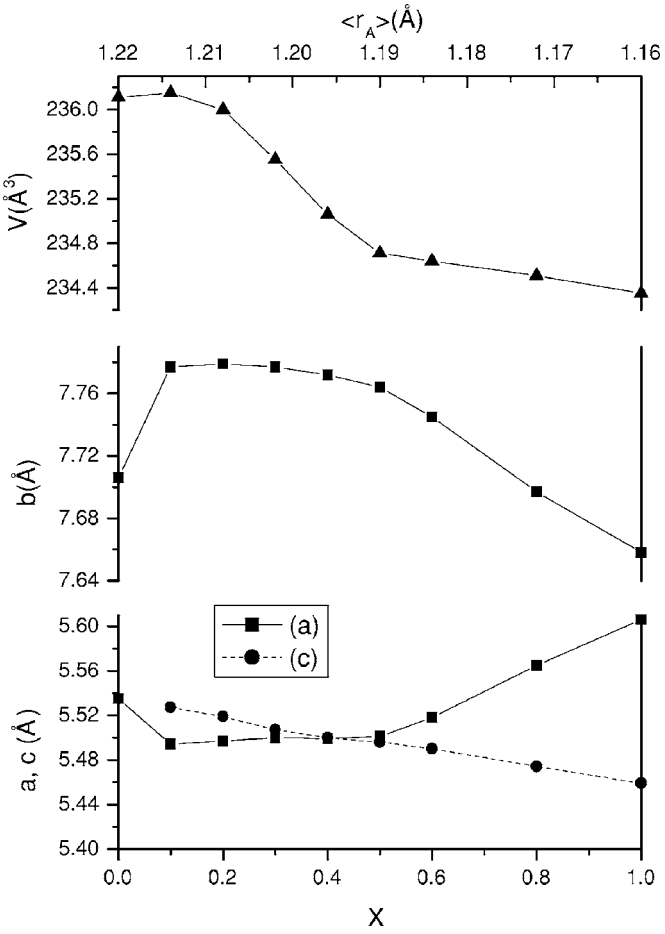

FIG. 3. Dependence of the lattice constants a, b, and c and the unit cell volume V on Pr content and on $\langle r_A \rangle$.

and c lattice parameters slightly change for $x=0.1-0.6$. Above 0.6, the a parameter increases while the b and c parameters decrease. The unit cell volume starts to increase with decreasing Pr near the transition from ORT-1 to ORT-2. In ORT-1 phase, the lattice parameter relations fulfill the criterion characteristic for a cooperative Jahn-Teller distortion of the MnO_6 octahedra superimposed on orthorhombic structure. The combination of a mismatch effect between (La,Pr)-O and Mn-O layers and a Jahn-Teller distortion promotes a different bond angles and lengths in the MnO_6 octahedra.

Neutron diffraction experiments were performed for the samples with $x=0.1$, 0.3, 0.6, 0.8, and 1.0. The data for the samples with $x=0.1$, 0.6, and 1.0 are shown in Fig. 4. An analysis of the neutron diffraction patterns in paramagnetic phase confirms the x-ray diffraction results. The calculations

TABLE I. Lattice and atomic positional parameters for the $La_{1-x}Pr_xMnO_3$ compounds at room temperature derived from x-ray data. Standard deviations are given in brackets. The atomic positions for La/Pr are 4*c* (x_R, 1/4, z_R); Mn, 4*b* (0,0,1/2); O1, 4*c* (x_{O1}, 1/4, z_{O1}); O2 8*d* (x_{O2}, y_{O2}, z_{O2}).

x	A (Å)	B (Å)	C (Å)	x_R	z_R	x_{O1}	z_{O1}	x_{O2}	y_{O2}	z_{O2}	R_{Bragg} (%)	R $(\%)_{wp}$
0.1	5.4941(7)	7.777(1)	5.5269(6)	0.0189(5)	−0.003(1)	0.489(6)	0.063(9)	0.262(10)	0.035(5)	0.732(9)	13.3	9.13
0.2	5.4971(8)	7.779(1)	5.5193(6)	0.0214(5)	−0.008(2)	0.490(6)	0.065(11)	0.287(11)	0.035(5)	0.739(7)	12.7	10.8
0.3	5.500(1)	7.777(3)	5.507(2)	0.0281(6)	−0.004(1)	0.483(7)	0.134(10)	0.274(10)	0.028(6)	0.763(5)	10.9	10.9
0.4	5.499(1)	7.772(1)	5.500(1)	0.0312(6)	−0.0057(5)	0.496(7)	0.135(9)	0.280(11)	0.017(6)	0.698(4)	10.9	12.5
0.5	5.5006(9)	7.764(1)	5.496(1)	0.0326(6)	−0.0071(7)	0.468(8)	0.102(8)	0.287(10)	0.012(6)	0.701(5)	9.8	9.62
0.6	5.5182(7)	7.745(1)	5.4903(8)	0.0381(8)	−0.0051(12)	0.472(7)	0.095(8)	0.272(6)	0.034(5)	0.719(7)	8.57	7.52
0.8	5.5652(5)	7.6974(8)	5.4744(6)	0.0401(5)	−0.0066(8)	0.464(6)	0.100(6)	0.282(5)	0.026(4)	0.726(6)	12.0	9.13
1	5.6061(5)	7.6581(7)	5.4586(6)	0.0466(4)	−0.0089(7)	0.473(5)	0.078(3)	0.295(3)	0.029(3)	0.716(5)	12.8	8.38

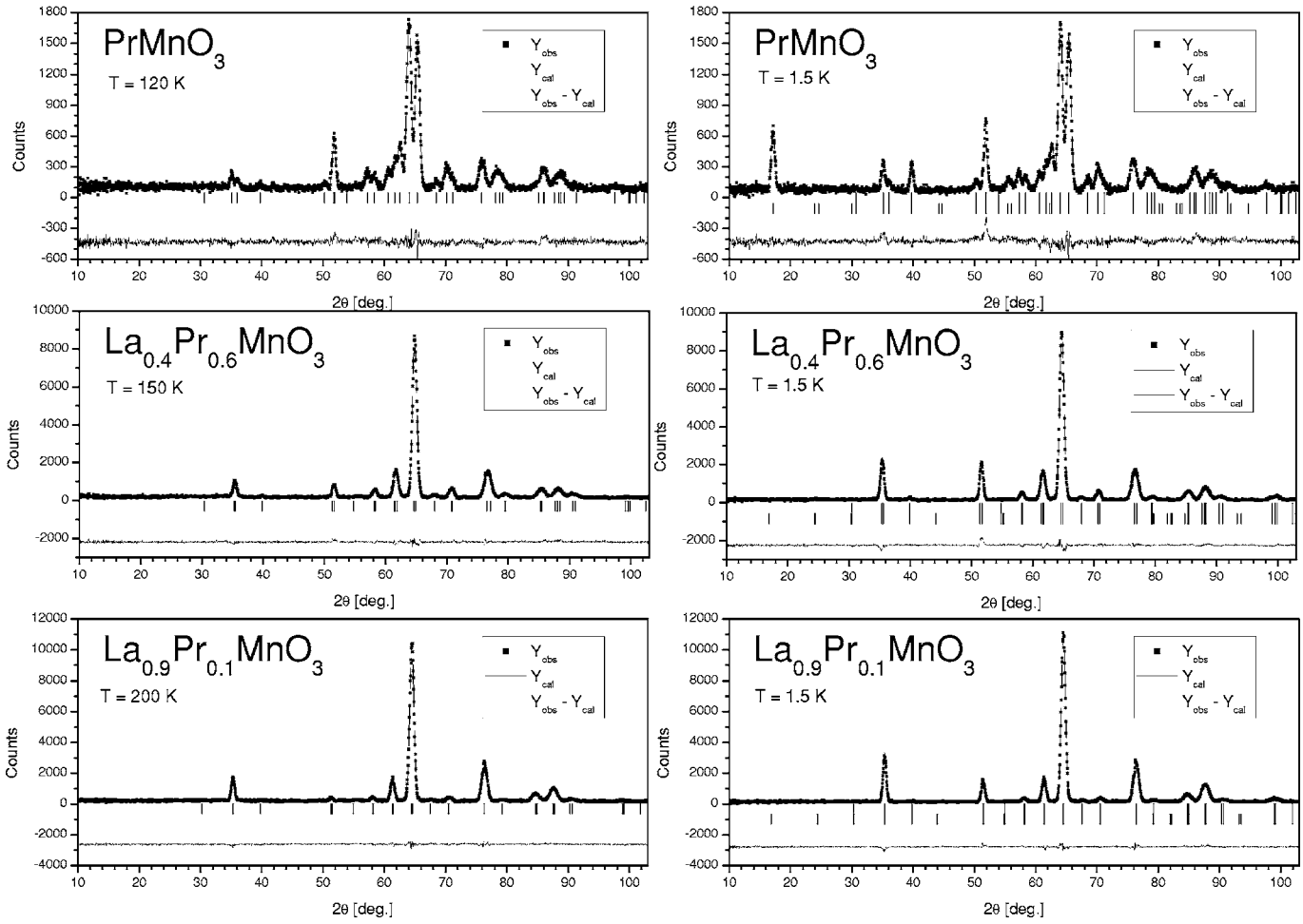

FIG. 4. Neutron diffraction patterns: observed (solid circles) and calculated (solid lines) for the $La_{1-x}Pr_xMnO_{3+\delta}$ compounds with $x=0.1$, 0.6, and 1.0. The right part of the figure shows the data recorded at 1.5 K and at the left part measured at temperatures 200, 150, and 120 K for the samples with $x=0.1$, 0.6, and 1.0, respectively. The ticks in the top row correspond to the nuclear Bragg reflections and the ones in the bottom row to the magnetic peaks. The difference between the observed and calculated patterns is shown at the bottom of each diagram.

of neutron diffraction patterns were performed assuming that the rare-earth sublattice is defected. The determined structural parameters, the occupation parameter of the rare-earth sublattice, and O1 and O2 positional parameters, refined on the basis of neutron diffraction patterns collected at different temperatures, are listed in Table II.

B. Magnetic properties

1. ac susceptibility

The $\chi'(T)$ dependences measured at ac field of 5.0 Oe with frequency of 48 Hz are presented in Figs. 5(a)–5(c). The real part of the ac susceptibility for $x=0-0.3$ rapidly

TABLE II. Crystal structure parameters of the $La_{1-x}Pr_xMnO_3$ compounds refined on the basis of neutron diffraction patterns collected at different temperatures, T_{meas}. Standard deviations are given in bracket. The atomic positions for La/Pr are 4*c* (x_R, 1/4, z_R); Mn, 4*b* (0,0,1/2); O1, 4*c* (x_{O1}, 1/4, z_{O1}); O2 8*d* (x_{O2}, y_{O2}, z_{O2}).

x	T_{meas}, K	A (Å)	B (Å)	C (Å)	x_R	z_R	x_{O1}	z_{O1}	x_{O2}	y_{O2}	z_{O2}	R_{Bragg} (%)
0.1	200 K	5.500(2)	7.788(4)	5.522(2)	0.0211(9)	0.007(4)	0.485(1)	0.071(2)	0.2833(8)	0.032(1)	0.743(2)	4.02
0.3	180 K	5.501(2)	7.774(3)	5.507(1)	0.0259(9)	0.010(3)	0.485(1)	0.075(2)	0.2881(9)	0.0320(8)	0.737(2)	4.91
0.6	150 K	5.507(2)	7.722(2)	5.480(2)	0.034(1)	0.001(4)	0.484(1)	0.072(2)	0.291(1)	0.0373(9)	0.725(2)	4.38
0.8	130 K	5.564(2)	7.673(3)	5.467(2)	0.042(1)	−0.004(2)	0.483(1)	0.073(1)	0.2961(7)	0.0402(6)	0.7175(9)	4.89
1	120 K	5.608(2)	7.634(3)	5.442(2)	0.050(2)	−0.049(2)	0.483(1)	0.077(2)	0.2999(8)	0.0412(7)	0.7148(9)	5.51

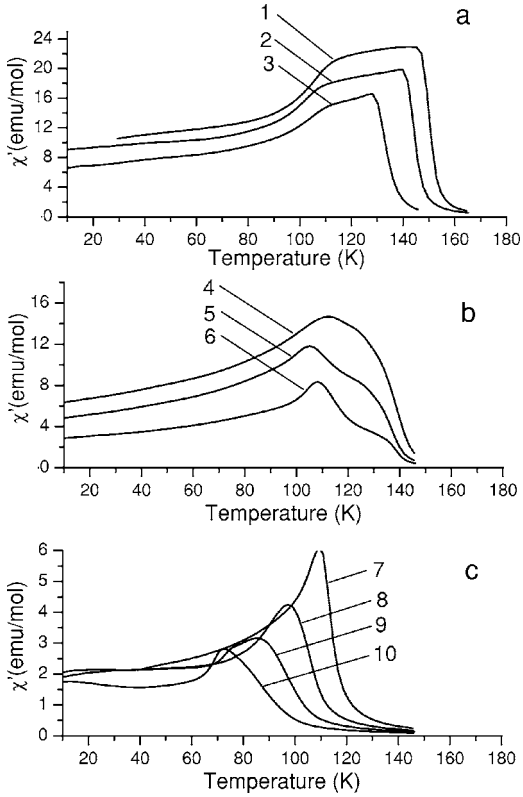

FIG. 5. Temperature dependence of the real part of ac magnetic susceptibility of $La_{1-x}Pr_xMnO_{3+\delta}$ compounds for $x=0.1,0.2,0.3$ (*a*, lines 1, 2, 3); for $x=0.4,0.5,0.6$ (*b*, lines 4, 5, 6); and for $x=0.7,0.8,0.9,1.0$ (*c*, lines 7, 8, 9, 10).

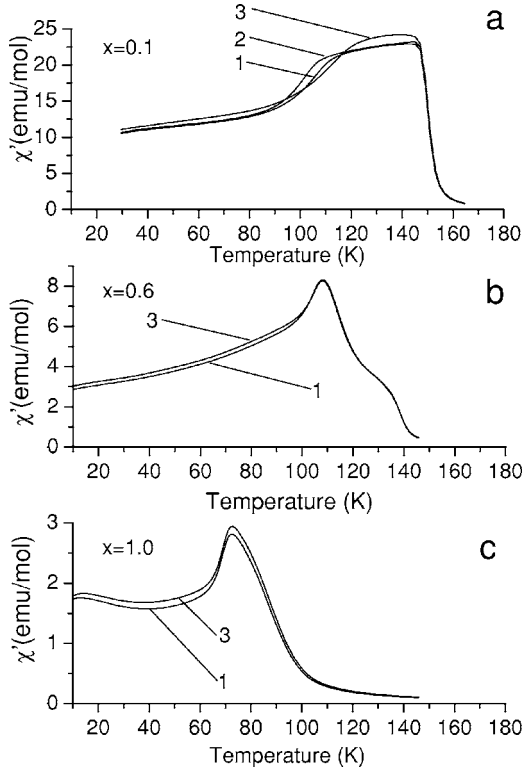

FIG. 6. Temperature dependence of the real part of *ac* magnetic susceptibility of $La_{1-x}Pr_xMnO_{3+\delta}$ compounds for $x=0.1$, 0.6, and 1.0 measured at frequencies of 48 (line 1), 500 (line 2), and 10 000 Hz (line 3).

develops below T_C ($T_C=153$ K for $x=0$) indicating the onset of FM component [Fig. 5(a)]. Next it flattens and starts to decrease with decreasing temperature at about 115 K. Such behavior may indicate an appearance of AFM component. For $x=0.4-0.6$ [Fig. 5(b)], the susceptibility curves demonstrate peculiarities different from behavior observed for $x<0.3$, namely, the phase transition interval around T_C is relatively broad and the $\chi'(T)$ dependences have both an inflection of curve just above T_C and maximum at $T\approx 115\div 108$ K. It is an indicative of the presence of ferromagnetic and antiferromagnetic components as well as of antiferromagnetism development at an expense of ferromagnetism. The $\chi'(T)$ curves for the samples with $x=0.7-1.0$ do not exhibit a ferromagnetic behavior, showing a sharp peak which shifts in temperature from 75 to 115 K with increasing x [Fig. 5(c)]. Such behavior of the $\chi'(T)$ dependences is supposed to be connected with the onset of magnetic canted structure below $T_{CANT}\approx 115$ K.

Other characteristic peculiarities of the ac susceptibility for the samples with $x=0.8-1.0$ are related to the weak temperature dependence of susceptibility in the temperature range from 60 down to 15 K and its decrease below 15 K. A small increase of $\chi'(T)$ dependence below 40 K observed for the sample with $x=1.0$ can be connected with Pr magnetic moments ordering. This agrees with the fact that Pr moments in $Pr_{0.9}MnO_3$ start to order below 50 K.[25] Another explanation of the increase in the susceptibility at 40 K can be connected with the depinning of magnetic domain walls.[16] It should be noted that the phase transition temperature does not shift with increasing frequency. As an illustration, Fig. 6 shows the $\chi'(T)$ susceptibility measured at frequencies of 48, 500, and 10 000 Hz for the samples with $x=0.1$, 0.6, and 1.0.

The temperature dependences of inverse susceptibility are linear at temperatures above T_C and they obey the Curie-Weiss law,

$$\chi_i = \chi_{0i} + \frac{C_i}{T-\theta_i},$$

where C_i is the Curie-Weiss constant, χ_{0i} is the background susceptibility, and θ_i is the Curie-Weiss temperature. The θ_i temperatures as a function of x are listed in Table III. A shift of inverse susceptibility to lower temperatures with decreasing $\langle r_A\rangle$ indicates a decrease of magnetic interactions between Mn moments.

The applied pressure has no effect on the character of $\chi'(T)$ dependence, and increases the susceptibility value. Figure 7 presents the $\chi'(T)$ dependence for the compound with $x=0$, 0.5, and 1.0 recorded at selected external pressures up to 1.5 GPa. The T_C and T_{CANT} temperatures change linearly with increasing pressure. The derivatives dT_C/dP and dT_{CANT}/dP are concentration dependent. The T_C, T_{CANT}, θ_i values (at $P=0$), dT_C/dP and dT_{CANT}/dP are listed in Table III.

TABLE III. The Curie temperature, T_C; paramagnetic Curie-Weiss temperature, θ; canted structure temperature, T_{CANT}; tolerance factor, t; magnetic moment, m; canted angle, γ; coercive field, H_{coerc}; remanent magnetization, M_{rem}; pressure coefficients of T_C (dT_C/dp) and of canted transition temperature (dT_{CANT}/dP); the Jahn-Teller distortion parameter, σ_{JT}; and the parameter w ($\sim$ electron bandwidth W) for the $La_{1-x}Pr_xMnO_{3+\delta}$ compounds.

X	0	0.1	0.2	0.3	0.4	0.5	0.6	0.7	0.8	0.9	1.0
T_C (K)	153	150	144	133	139	137	138	113	—	—	—
θ (K)	153	150	144	132	131	136	135	112	105	95	88
T_{CANT} (K)	115	115	112	113	113	106	108	108	97	86	73
t	0.963	0.961	0.958	0.956	0.953	0.951	0.948	0.946	0.943	0.941	0.939
m (μ_B/Mn)	3.2	3.4	3.5	3.6	3.2	3.3	2.9	2.9	2.7	2.2	1.7
γ (°)	32	26	21	16	31	29	39	39	45	55	70
H_{coerc} (kOe)	0.06	0.05	0.06	0.01	0.05	0.08	0.06	0.21	0.33	0.49	0.88
M_{rem} (emu/g)	3.3	2.6	2.8	0.5	1.50	2.8	2.0	7.5	11.0	15.6	16.6
dT_C/dp (K/Gpa)	5.6	2.9	2.9	2.9	2.7	2.5	2.7	—	—	—	—
dT_{CANT}/dp (K/Gpa)	−6.9	−6.2	−5.6	−5.1	−4.9	−5.7	−2.7	+0.5	+1.3	+2.9	+1.9
$\sigma_{JT}\times 10^2$ (Å)	—	1.92	1.75	1.43	1.36	6.41	6.86	—	7.25	—	7.18
$w\times 10^2$ (Å$^{-3.5}$)	—	9.16	9.21	9.12	9.08	9.04	8.93	—	8.90	—	8.89

2. dc magnetization

The field-cooled (FC) and zero-field-cooled (ZFC) magnetization recorded in magnetic field of 50 Oe for different Pr concentration are shown in Fig. 8. It is seen that $M(T)$ dependences are strongly influenced by the Pr content. For samples with $x<0.4$, the ferromagneticlike behavior is observed. Near transition temperature, the FC magnetization begins to rise sharply with decreasing temperature, indicating the onset of ferromagnetic ordering, and tends to the saturation with no further changes at low temperature. As Pr content increases above 0.4, a strong change in temperature evolution of magnetization is observed, namely, FC magnetization continuously increases as temperature decreases, without reaching the saturation at low temperatures, and the $M_{ZFC}(T)$ curves have a pronounce cusp in low fields at T_{CANT} which decreases as Pr concentration increases. The T_{CANT} temperature presumably is a temperature below which the collinear orientation of spins in Mn sublattice is disrupted.

A peculiarity of $M(T)$ dependences is the difference between FC and ZFC magnetization at low temperatures. The ZFC and FC magnetization curves for the samples with x

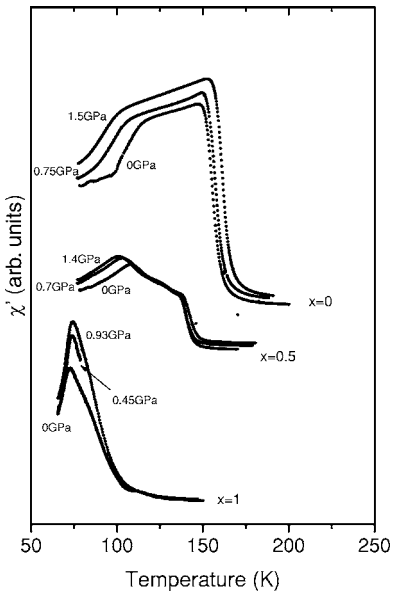

FIG. 7. Temperature dependence of the real part of ac magnetic susceptibility of $La_{1-x}Pr_xMnO_{3+\delta}$ compounds for $x=0$, 0.5, and 1.0 at some chosen values of the external pressure.

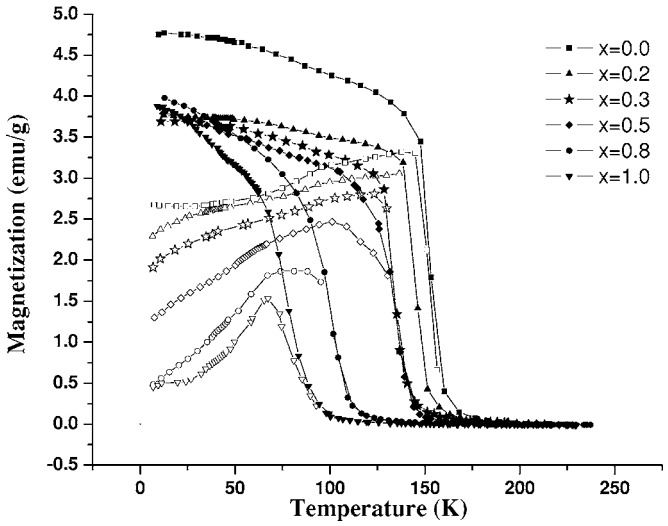

FIG. 8. Temperature dependence of FC magnetization (full symbols) and ZFC magnetization (open symbols) for different Pr concentrations in magnetic field of 50 Oe.

<0.5 begin to diverge just below T_C. For the samples with $x>0.5$, ZFC and FC magnetization curves start to separate above the phase transition temperature. The M_{FC}/M_{ZFC} ratio (at $T=4.2$ K and $H=50$ Oe) increases with increasing Pr content. The difference between FC and ZFC magnetization diminishes in magnetic field and disappears at $500 \div 1000$ Oe.

The FM phase transition temperature defined as the inflection point of $M(T)$ dependence was found to change nonmonotonously with increasing x (Table III). It decreases rapidly for $x<0.3$ and for $x>0.6$ and is independent on Pr concentration for $0.3<x<0.6$. The $T_C(x)$ and $\theta(x)$ dependences coincide practically. The changes of T_C are very well correlated with the Jahn-Teller distortion of the structure when $\langle r_A \rangle$ decreases. The low temperature behavior of magnetization for the end compositions ($LaMnO_3$ and $PrMnO_3$) should corresponds to an antiferromagnetic ordering. Nevertheless, in the $La_{1-x}Pr_xMnO_{3+\delta}$ samples with $x=0$ and 1.0 some deviations from such magnetic structure are observed. The distinction of $T_C \approx 155$ K at $x=0$ from usually observed temperature of AFM ordering ($T_N=140$ K) in $LaMnO_3$ is presumed to be due to a small excess of oxygen which results in cation vacancies or due to an effect connected with the depinning of magnetic domain walls as described in Ref. 16. The studies of the influence of the oxygen content on magnetic properties of $LaMnO_{3+\delta}$ have shown that the AFM ordering found in $LaMnO_3$ evolves towards a ferromagnetic order and T_C increases as δ increases.[30–33]

Magnetization dependences $M(T)$ in various magnetic fields and $M(H)$ isotherms have been measured as well. The transitions to paramagnetic state in magnetic field become broader, and the $M(T)$ dependences shift towards high temperatures, stabilizing the FM state. The magnetization isotherms for the samples with $x<0.4$ display a ferromagnetic-like behavior and do not change practically above 5–7 kOe. The behavior of the isotherms for Pr-rich compounds ($x>0.5$) differs from the typical FM behavior, and no sign of saturation is present in magnetic field up to 12 kOe (Fig. 9). The spontaneous magnetization determined by extrapolation of high field magnetization to $H=0$ gives a ferromagnetic component and allows us to estimate the canting angle. The magnetic moment of the Mn ion determined from magnetization changes from 3.2 ($x=0$) to 1.7 μ_B/Mn ($x=1.0$) passing through maximum (3.6 μ_B/Mn) at $x=0.3$ [inset (a) to Fig. 9]. The magnetic moments listed in Table III refer to the helium temperature. The sample with $x=0.9$ has a magnetic moment of ~ 2.2 μ_B/Mn that is comparable with the value of 2.72 μ_B/Mn obtained for $Pr_{0.9}MnO_3$.[25] Due to an absence of a fully ordered magnetic state obtained magnetic moments are small and this indicates that a part of the spins does not contribute to the collinear magnetic ordering. A decreasing magnetic moment indicates the weakening of DE FM interactions with respect to the AFM superexchange interactions and is also an indication of the canted spin configuration. The canting angle estimated decreases from 32° for $x=0$ to 16° for $x=0.3$ and then increases to 70° for $x=1$ [inset (b) to Fig. 9].

The hysteresis loops measured for all the studied samples in applied magnetic field up to 12 kOe at 4.2 K (Fig. 10) show that both coercive field (H_C) [inset (a) to Fig. 10] and remanent magnetization (M_{rem}) [inset (b) to Fig. 10] slightly change for $x \leqslant 0.6$ and for x above 0.6 abruptly increase from 0.06 to 0.88 kOe and from 2.0 to 16.6 emu/g, respectively. An increase of H_C coincides with an occurrence of a sharp peak in susceptibility at $x=0.7$. One can conclude that an increase of coercive field is mainly due to increase of the magnetic anisotropy resulting from the fact that Pr compounds are more anisotropic compared to La compounds. The increase of area under loop can be a result of an increase of the Jahn-Teller distortion of MnO_6 octahedra with Pr doping.

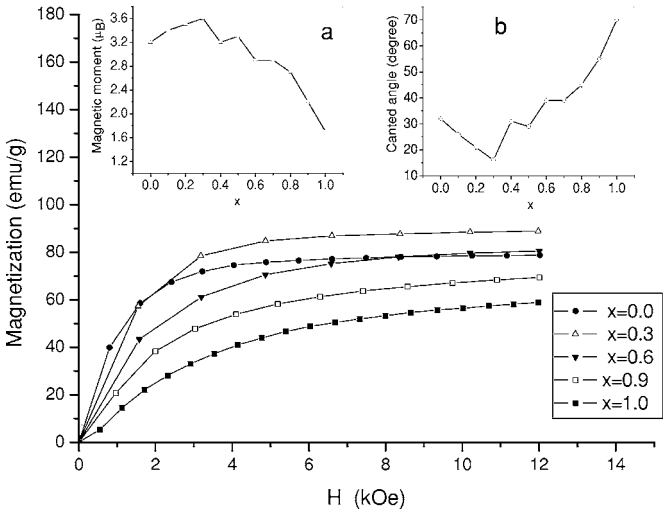

FIG. 9. $M(H)$ isotherms for different Pr concentration at $T=4.2$ K; the magnetic moment of Mn ion at 4.2 K (inset a) and the canted angle (inset b) as a function of x.

3. Neutron powder diffraction

The neutron powder diffraction data have allowed to clarify the character of magnetic interactions as a function of

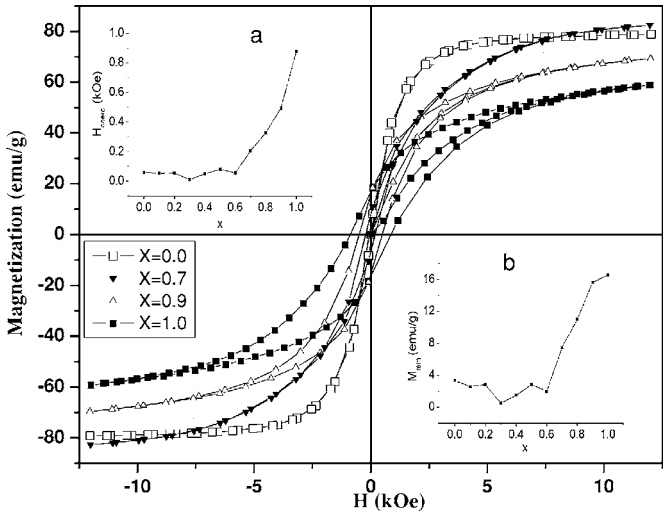

FIG. 10. Hysteresis loops as a function of magnetic field for different Pr concentrations in applied magnetic field up to 12 kOe at 4.2 K. Concentration dependences of coercive field (inset a) and remanent magnetization (inset b).

Pr concentration. The performed group theory analysis after Bertaut[34] gives us a possibility to establish the magnetic structure in the studied compounds. In these samples Mn atoms occupy the following positions in the crystallographic unit cell: Mn1 (0,0,1/2), Mn2 (1/2,0,0), Mn3 (0,1/2,1/2), and Mn4 (1/2,1/2,0). According to Bertaut's theory of spin transformation for the 4(c) site in the *Pnma* space group there are four magnetic structures possible: three antiferromagnetic (described by the vectors $\mathbf{G}=S_1-S_2+S_3-S_4$, $\mathbf{C}=S_1+S_2-S_3-S_4$, and $\mathbf{A}=S_1-S_2-S_3+S_4$), and one ferromagnetic ($F=S_1+S_2+S_3+S_4$).

The neutron diffraction patterns of the samples with $x=0.1$, 0.3, and 0.6 collected at 1.5 K are similar and show an increase in intensities of reflexes connected with the ferromagnetic ordering in the Mn sublattice as temperature decreases (Fig. 4). On the other hand, the intensities of these reflexes decrease as Pr content increases, what is connected with a decrease of ferromagnetic component. The refinement of the magnetic peaks intensities shows that the magnetic moments are parallel to the *b* axis and are equal to 3.34(4) μ_B for the samples with $x=0.1$ and 0.3 and to 3.15(4) μ_B for that one with $x=0.6$. This type of magnetic ordering is stable below T_C equal to 150, 135, and 126 K for the samples with $x=0$, 0.3, and 0.6, respectively, which is in good agreement with the results of magnetic measurements. A different distribution of magnetic peaks is observed in the patterns collected for the samples with $x=0.8$ and 1.0. Except the peaks corresponding to the FM phase there are additional peaks, for example, (010) at $2\theta=17.1°$ in Fig. 4 (for the sample with $x=1.0$), which indicates existence of an antiferromagnetic component. The refinement of the neutron diffraction data at 1.5 K shows that in these compounds the magnetic ordering of the C_xF_y type occurs with the following components of the magnetic moments: $\mu_x=1.95(3)$ μ_B and $\mu_y=1.56(6)$ μ_B and the total moment equal to 2.50(5) μ_B for the sample with $x=1.0$ and $\mu_x=1.14(2)$ μ_B and $\mu_y=2.30(4)$ μ_B and the total moment equal to 2.57(4) μ_B for that one with $x=0.8$. The magnetic peak intensities are temperature independent up to 70 K for the sample with $x=1.0$ and up to 100 K for that one with $x=0.8$.

IV. DISCUSSION

The detailed measurements performed on a series of $La_{1-x}Pr_xMnO_{3+\delta}$ compounds have allowed to clarify some interesting aspects related to the strong influence of the size effect on their structural properties and magnetic ground state. The x-ray and neutron diffraction data show that the crystal structure undergoes the concentration-induced transition from rhombohedral unit cell towards orthorhombic one with a small Jahn-Teller distortion between $x=0$ and $x=0.1$ and then towards highly distorted orthorhombic unit cell above $x=0.6$. Using the lattice parameters the interatomic Mn-Mn and Mn-O distances and Mn-O-Mn angles both along the *b* axis and in the *ac* plane were calculated and are presented in Fig. 11. For the samples with $x\leqslant 0.5$, the interatomic Mn-Mn distances in the *ac* plane and between the plane ($y=0$ and 1/2) are equal in the limit of the experimental error, but the difference between them increases with increasing *x*. Similar dependence is observed for the Mn-O distances and Mn-O-Mn angles. In the MnO_6 octahedra there is one long Mn-O bond (>2.0 Å) and two short ones (<2.0 Å), which reveal the presence of the Jahn-Teller distortion. The Mn-O-Mn bond angles differ significantly from 180° implying strong distortion of the perovskite structure through the tilting of the MnO_6 octahedra. Knowing Mn-O and an average ⟨Mn-O⟩ bond lengths from the x-ray diffraction data at room temperature, the coherent Jahn-Teller distortions were determined using the relation[35]

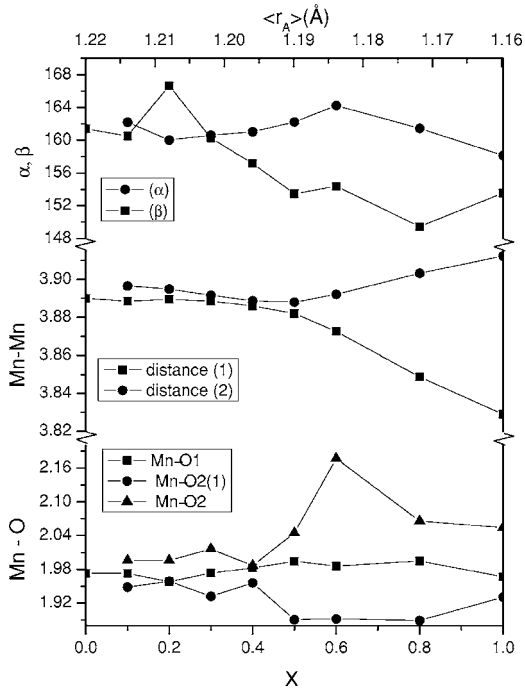

FIG. 11. Interatomic Mn-Mn (1 and 2) and Mn-O distances and Mn-O-Mn bond angles (α and β) as a function of *x* and $\langle r_A\rangle$. The α and β angles and the 1 and 2 distances are along the *b* axis and in the *ac* plane, respectively.

$$\sigma_{JT}=\sqrt{1/3\sum_i[(Mn\text{-}O)_i-\langle Mn\text{-}O\rangle]^2}.$$

The calculated Jahn-Teller distortion parameters, σ_{JT}, for all the samples are very small and they are typical for the compounds with the orthorhombic *Pnma*-type structure (Table III).

In parallel with the changes in the crystallographic structure remarkable magnetic ordering effects were found. Each series of samples displays quite different magnetic properties depending on the average *A*-site ionic radius. A weakening of FM interactions and an enhancement of AFM ones were observed with decreasing $\langle r_A\rangle$. The peculiarities of both susceptibility and magnetization for $x<0.7$ in temperature interval from T_C to $T_{CANT}\approx 108\div 115$ K (Figs. 5 and 8) indicate an appearance of AFM component. However, the neutron diffraction data do not show the presence of antiferromagnetic component for these compositions. Similar situation was reported in Ref. 19 when the existence of the cusp in ZFC magnetization observed in $Pr_{0.7}Ca_{0.3}MnO_3$ was explained as

a spin-glasslike behavior that did not correlate with the results of neutron studies. It can result from the fact that the reflexes connected with AFM component are of very small intensity. From the magnetic data, it is clear that the AFM component of magnetic moment is small and, for example, for canted angle of 16° equal to 0.6 μ_B. The absence of the reflexes corresponding to the AFM component in the neutron diffraction patterns for samples with x equal to 0.1, 0.3, and 0.6 can be supposed to be connected with the fact that these components do not form long range ordering but rather random angular magnetic structure, which cannot be observed with a neutron diffraction method.[36–38] In this range of Pr concentrations and temperatures, FM interactions of the F_y type are established to be dominant and to coexist with the AFM ones. The $\chi'(T)$ and $M(T)$ results show that the small $\langle r_A \rangle$ favors the canted state. Indeed, in Pr-rich region the occurrence of a canted magnetic arrangements of the C_xF_y type is confirmed by the neutron diffraction data, which show that the interlayer antiferromagnetic superexchange exceeds the FM DE. This magnetic order can be ascribed as the canted antiferromagnetic one.[39] The C_xF_y type magnetic structure appearing for $x \geqslant 0.7$ has been also observed for defected $Pr_{0.9}MnO_3$.[25] A similar character of magnetic ordering is suggested to result from a competition between ferromagnetic and antiferromagnetic interactions, giving rise to distorted low temperature system with spin canted features. The Dzyaloshinskii-Moriya interaction can also take place in these manganites; however, it is insignificant as compared with competitive DE and superexchange interactions, which yield a canted structure observed.

The T_C and θ temperatures nonmonotonously decrease with increasing x. The concentration-independent $T_C(\langle r_A \rangle)$ relation at $0.3 < x < 0.6$ is presumably due to both a small A-cation size disorder and a constancy of Mn-Mn distance in this interval of x. It indicates that the influence of Mn-Mn and Mn-O distances on the transition temperature is stronger than the change of Mn-O-Mn angle that is in an agreement with Ref. 3.

The magnetic properties of $La_{1-x}Pr_xMnO_{3+\delta}$ can be interpreted in terms of both the average ionic radius $\langle r_A \rangle$ (or equivalently the tolerance factor) and the variance σ^2 characterizing a local distortion of the A-cation site. The studies show that the variance σ^2 equal to 3.4×10^{-4} Å^2 is the crucial value for an occurrence of spin canting state. The T_C is shown to decrease with both increasing and decreasing σ^2, unlike in the Ca-doped manganites, where an increasing σ^2 diminishes the phase transition temperature.[1,4] In our case, the A-cation variance is small (σ^2 is of the order of 10^{-4} Å^2) and the variation of phase transition temperature is mostly connected with the changes in $\langle r_A \rangle$.

Since Pr has a smaller ion radius than La, the Pr substitution reduces the tolerance factor (Table III) and enhances a lattice distortion of oxygen octahedra. The MnO_6 octahedra tilt and rotate in order to fill the extra space around the A site and to optimize the A-O bond length that implies smaller Mn-O-Mn bond angle. In the frame of the DE interaction model,[13,14] the decrease of the Mn-O-Mn angle and of the average ⟨Mn-O⟩ distances diminishes the electron bandwidth. It also hinders Mn-e_g electron hopping that should weaken the double-exchange along the b axis with respect to the superexchange interactions in the ac plane and should decrease the magnetic ordering temperature, as it is observed in the current studies. The decreasing ratio of the ferro- and antiferromagnetic components with increasing x favors occurrence of the canted spin structure. In the studied samples, the nonstoichiometry induces the presence of Mn^{4+} ions with holes in the e_g band. In the $Pr_{1-x}M_xMnO_3$ (M=Ca, Sr, Ba) systems the canted arrangement is shown to exist when the content of the Mn^{4+} ions is in the range of 5–15%.[12] This is in a good agreement with a number of vacancies in the rare-earth sublattice determined from the neutron diffraction experiments.

The ac magnetic susceptibility measurements under external pressure have allowed us to establish the pressure effect on the magnetic ordering temperatures in the studied series of compounds. The largest value of dT_C/dP was obtained for the sample with the rhombohedral crystal structure (x=0). The dT_C/dP values determined for the other samples are considerably smaller than those reported for $La_{1-x}Ca_xMnO_3$ manganites, in which the double-exchange interaction is dominant.[40] This suggests rather small influence of the external pressure on the interatomic distances and, in consequence, on the magnetic interactions. In the $La_{1-x}Pr_xMnO_{3+\delta}$ series, the T_C slightly increases with increasing external pressure while it decreases with decreasing unit cell volume. The origin of this unusual behavior is not clear. It is worth noting (Table III) that in the concentration range $0 \leqslant x \leqslant 0.6$ the significant change in the unit cell volume corresponds to small change in the Curie temperature (ΔT_C=15 K, i.e., about 10%), while for higher x values, a very small change in the unit cell volume is accompanied by a huge decrease in the Curie temperature (ΔT_C=50 K, i.e., about 40%). In perovskite compounds, within tight binding approximation, the electron bandwidth W depends on the bond lengths and angles through the overlap integrals between the 3d orbital of Mn atoms and 2p orbital of O atom. The following empirical formula has been used to describe this dependence:[41]

$$W \sim w = \cos \omega / \langle d_{\text{Mn-O}} \rangle^{3.5},$$

where the angle $\omega = 1/2(\pi - \langle \text{Mn-O-Mn} \rangle)$. The w values calculated for x between 0.1 and 1.0, using the x-ray diffraction data obtained at room temperature, decrease slowly with increasing x (Table III). The internal structural parameters are connected with the magnetic ordering temperature by the relation $W(d_{\text{Mn-O}}, \omega)$. The obtained results clearly confirm this dependence.

On the basis of experiments performed a magnetic phase diagram of $La_{1-x}Pr_xMnO_{3+\delta}$ is constructed and is schematically shown in Fig. 12. It contains three different magnetic phases, namely, paramagnetic phase (above T_C); ferromagnetic state of the F_y type for the Pr content $x < 0.7$ in the temperature interval from T_C to T_{CANT} and canted spin arrangement of C_xF_y type below T_{CANT}. It should be noted that whereas a paramagnetic-ferromagnetic-spin canted phase transition takes place for the samples with $x < 0.7$, then for higher Pr concentration, $x > 0.7$, the transition from paramagnetic to spin canted state is observed. A presence of cusp in both M_{ZFC} magnetization and $\chi(T)$ dependence and an ab-

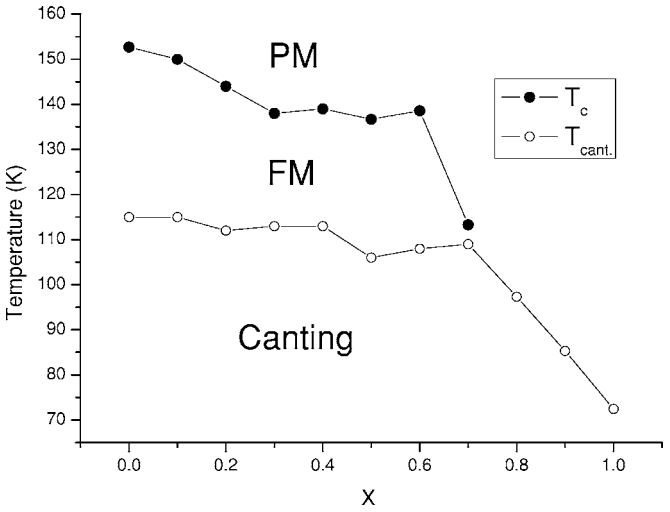

FIG. 12. Magnetic T-x phase diagram.

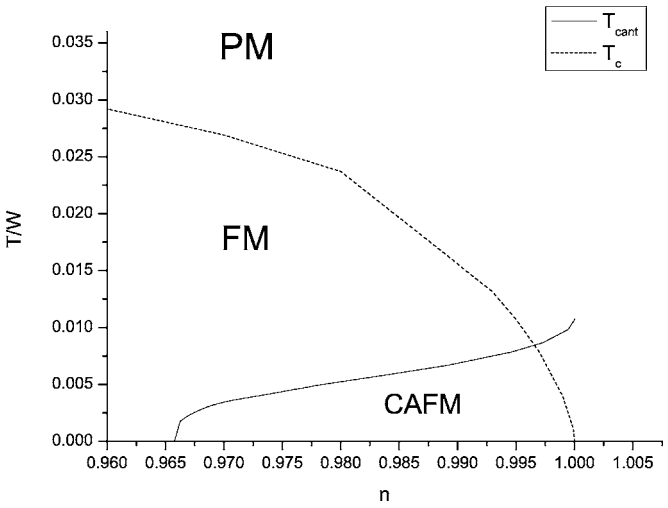

FIG. 13. Calculated phase diagram T/W vs n, where W is the electron bandwidth and n is the carrier concentration.

sence of frequency dependence of the phase transition temperature are a characteristic feature of spin canted magnetic structures. The occurrence of a canted spin arrangement at T_{CANT} is confirmed by neutron diffraction data.

Let us consider the competition between DE and superexchange (SE) interactions in detail. We consider parameters determining the thermodynamics of $PrMnO_3$ manganite, namely, J_1 and J_2 which characterize the FM intra- and AFM interplane superexchange, respectively, and W is the bandwidth of e_g electrons with concentration n. According to Ref. 42, in $PrMnO_3$ the J_1 and J_2 parameters are equal to 6.85 K and −7 K, respectively, and then the parameter $d=J_2/2J_1=-0.51$. The Neel temperature, T_N, is expressed as $T_N/4J_1=2/3[S(S+1)(1-d)]$, where the spin $S=2$ for Mn^{3+}. For $PrMnO_3$, the calculated T_N is equal to 112 K. In our measurements we obtain T_N equal to 73 K for $PrMnO_{3+\delta}$. The difference between calculated and experimental values is related to the fact that in the mean field approximation the spin fluctuations were not taken into account. A distinction of the Neel temperatures for Pr-containing specimens is supposed to be also caused by different content of vacancies. These vacancies lead to frustration of magnetic moments and consequently to decrease of superexchange interactions and to decrease of the Néel temperature. For quantitative analysis of experimental phase transitions and for construction of theoretical phase diagram T/W versus n (Fig. 13), we have used the results of analysis of the phase transitions in $(La_{0.7}Ca_{0.3})_{1-x}Mn_{1+x}O_3$ with parameters $d=-0.3$, $J_1=9.6$ K, and $W=1$ eV.[43]

The important peculiarity of calculated diagram is a narrow area near $n\sim1$ (hole concentration $1-n\sim0.003$), in which the PM-canted spin phase transition is realized. This follows from the fact that T_C tends to zero at $n\rightarrow1$ and T_{CANT} is finite at $n=1$. This is in an agreement with experiment data. Indeed, as it is seen in Fig. 12, for the samples with $x\geqslant0.7$ only one transition PM-canted phase is observed.

V. CONCLUSIONS

Magnetic, x-ray, and neutron powder diffraction investigations on polycrystalline $La_{1-x}Pr_xMnO_{3+\delta}$ ($x=0-1.0$) manganites have been carried out. The magnetic properties, crystallographic symmetry, and the phase transition temperatures are shown to depend strongly upon the average A-cation radius caused by Pr substitution for La. The $La_{1-x}Pr_xMnO_{3+\delta}$ manganites have the following crystal structure: rhombohedral (space group $R\,\bar{3}c$) for $x=0$, orthorhombic with small Jahn-Teller distortion for $0.1<x<0.6$, and highly distorted orthorhombic ($Pnma$) modifications for $x>0.6$. The lattice parameters, the Mn-Mn and Mn-O interatomic distances slightly change for the samples with $x<0.6$, but the difference between them increases with increasing x. The Mn-O-Mn bonding angles are smaller than 180°, implying strong distortion of the MnO_6 octahedra. The samples with $x<0.4$ show a ferromagneticlike behavior below T_C, for $x>0.4$ the ferromagnetic interactions diminish with respect to the AFM superexchange interactions, and the magnetic properties begin to manifest the peculiarities characteristic for the canted spin structure. At low temperatures, the canted ordering exists and the canted angle increases with increasing Pr content. The magnetic phase diagram illustrating the concentration dependence of the phase transition temperature was constructed. The different magnetic states were established, namely, paramagnetic phase (above the T_C); ferromagnetic state of the F_y type for $x<0.7$ in temperature range from T_C to $T_{CANT}\approx108\div115$ K and the phase with a canted spin arrangement of the C_xF_y type below the T_{CANT} temperature. For samples with $x<0.7$, the change of the magnetic structure from ferromagnetic to the canted one is observed with decreasing temperature, while for $x>0.7$ the direct transition from paramagnetic to spin canted state takes place. The results are interpreted taking into account the competition of ferromagnetic double-exchange and antiferromagnetic superexchange interactions. This competition leads to the low temperature disordered system with spin canted features as a result of a decrease of the average A-site cation radius.

ACKNOWLEDGMENTS

This work was in part supported by the Polish Govern-

ment Agency KBN (Project No. 1 P03B 025 26), by the Russian Foundation for Basic Research (Grant No. 04-02-17598) and was financed by the Polish Ministry of Education and Science as a Targeted Research Project, over the period 2005–2008 (Project PBZ-KBN-115/T08/01). The authors would like to express their gratitude to N. A. Doroshenko and Z. F. Kravchenko for preparation and characterization of the samples. Two of us (S. B. and E. W.) would like to express our gratitude to the management of the Berlin Neutron Scattering Center for their financial support and kind hospitality. The neutron diffraction studies at Hahn-Meitner-Institut were supported by the European Commission under the 6th Framework Programme through the Key Action: Strengthening the European Research Area, Research Infrastructures, Contract No. RII3-CT-2003-505925 (NMI3).

*To whom correspondence should be addressed: e-mail dyakon@ifpan.edu.pl;

[1] L. M. Rodriguez-Martinez and J. P. Attfield, Phys. Rev. B **54**, R15622 (1996).
[2] C. Martin, A. Maignan, M. Hervieu, and B. Raveau, Phys. Rev. B **60**, 12191 (1999).
[3] P. G. Radaelli, G. Iannone, M. Marezio, H. Y. Hwang, S. W. Cheong, J. D. Jorgensen, and D. N. Argyriou, Phys. Rev. B **56**, 8265 (1997).
[4] F. Damay, Z. Jirak, M. Hervieu, C. Martin, A. Maignan, B. Raveau, G. Andre, and F. Bouree, J. Magn. Magn. Mater. **190**, 221 (1998).
[5] H. Y. Hwang, S. W. Cheong, P. G. Radaelli, M. Marezio, and B. Batlogg, Phys. Rev. Lett. **75**, 914 (1995).
[6] R. Mahesh, R. Mahendiran, A. K. Raychaudhuri, and C. N. R. Rao, J. Solid State Chem. **120**, 204 (1995).
[7] F. Damay, C. Martin, A. Maignan, and B. Raveau, J. Appl. Phys. **82**, 6181 (1997).
[8] A. Maignan, C. Martin, G. Van Tendeloo, M. Hervieu, and B. Raveau, Phys. Rev. B **60**, 15214 (1999).
[9] E. O. Wollan and W. C. Koehler, Phys. Rev. **100**, 545 (1955).
[10] G. H. Jonker, Physica (Amsterdam) **22**, 707 (1956).
[11] F. Moussa, M. Hennion, J. Rodriguez-Carvajal, H. Moudden, L. Pinsard, and A. Revcolevschi, Phys. Rev. B **54**, 15149 (1996).
[12] Z. Jirak, J. Hejtmanek, E. Pollert, M. Marysko, M. Dlouha, and S. Vratislav, J. Appl. Phys. **81**, 5790 (1997).
[13] C. Zener, Phys. Rev. **81**, 440 (1951).
[14] P. G. de Gennes, Phys. Rev. **118**, 141 (1960).
[15] Z. Jirak, S. Krupicka, Z. Simsa, M. Dlouha, and S. Vratislav, J. Magn. Magn. Mater. **53**, 153 (1985).
[16] P. Duan, Z. Chen, S. Dai, Y. Zhou, H. Lu, K. Jin, and B. Cheng, Appl. Phys. Lett. **84**, 4741 (2004).
[17] P. G. Radaelli, M. Marezio, H. Y. Hwang, and S. W. Cheong, J. Solid State Chem. **122**, 914 (1996).
[18] A. Maignan, Ch. Simon, V. Caignaert, and B. Raveau, Z. Phys. B: Condens. Matter **99**, 305 (1996).
[19] A. Maignan, U. V. Varadaraju, F. Millange, and B. Raveau, J. Magn. Magn. Mater. **168**, L237 (1997).
[20] P. S. A. Kumar, P. A. Joy, and S. K. Date, Solid State Commun. **108**, 67 (1998).
[21] Y. Tomioka, A. Asamitsu, Y. Moritomo, H. Kuwahara, and Y. Tokura, Phys. Rev. Lett. **74**, 5108 (1995).
[22] H. Fujishiro, M. Ikebe, S. Ohshiden, and K. Noto, J. Phys. Soc. Jpn. **69**, 1865 (2000).
[23] M. Uehara, S. Mori, C. H. Chen, and S.-W. Cheong, Nature **399**, 560 (1999).
[24] A. M. Balagurov, V. Yu. Pomjakushin, D. V. Sheptyakov, V. L. Aksenov, P. Fischer, L. Keller, O. Yu. Gorbenko, A. R. Kaul, and N. A. Babushkina, Phys. Rev. B **64**, 024420 (2001).
[25] A. Munoz, J. A. Alonso, M. J. Martinez-Lope, and M. T. Fernandez-Diaz, Solid State Commun. **113**, 227 (2000).
[26] R. D. Shannon, Acta Crystallogr., Sect. A: Cryst. Phys., Diffr., Theor. Gen. Crystallogr. **32**, 751 (1976).
[27] J. Carvajal-Rodriguez, Physica A **192**, 55 (1993).
[28] C. Ritter, M. R. Ibarra, J. M. De Teresa, P. A. Algarabel, C. Marguina, J. Blasco, J. Garcia, S. Oseroff, and S.-W. Cheong, Phys. Rev. B **56**, 8902 (1997).
[29] B. C. Hauback, F. Helmer, and N. Sakai, J. Solid State Chem. **124**, 43 (1996).
[30] J. Topfer and J. B. Goodenough, J. Solid State Chem. **130**, 117 (1997).
[31] R. Laiho, K. G. Lisunov, E. Lahderanta, P. A. Petrenko, J. Salminen, V. N. Stamov, Yu. P. Stepanov, and V. S. Zakhvalinskii, J. Phys. Chem. Solids **64**, 2313 (2003).
[32] J. A. Alonso, M. J. Martinez-Lope, M. T. Casais, and M. Munoz, Solid State Commun. **102**, 7 (1997).
[33] J. A. M. Van Roosmalen, E. H. P. Cordfunke, R. B. Helmholdt, and H. W. Zandbergen, J. Solid State Chem. **110**, 100 (1994).
[34] E. F. Bertaut, Acta Crystallogr., Sect. A: Cryst. Phys., Diffr., Theor. Gen. Crystallogr. **24**, 217 (1968).
[35] S. Quezel-Ambrunaz, Bull. Soc. Fr. Mineral. Cristallogr. **91**, 339 (1968).
[36] K. P. Belov, *Ferrites in Strong Magnetic Fields* (Nauka, Moscow, 1972).
[37] S. Nizioł, Phys. Status Solidi A **16**, 555 (1973).
[38] J. J. Bara, A. T. Pędziwiatr, Z. M. Stadnik, A. Szytuła, J. Todorović, Z. Tomkowicz, and W. Zarek, Phys. Status Solidi A **44**, 325 (1977).
[39] A. J. Millis, Nature **392**, 147 (1998).
[40] J. J. Neumeier, M. F. Hundley, J. D. Thompson, and R. H. Heffner, Phys. Rev. B **52**, R7006 (1995).
[41] M. Medarde, J. Mesot, P. Lacorre, S. Rosenkranz, P. Fischer, and K. Gobrecht, Phys. Rev. B **52**, 9248 (1995).
[42] L. E. Gontchar and A. E. Nikiforov, Phys. Rev. B **66**, 014437 (2002).
[43] E. Zubov, V. Dyakonov, and H. Szymczak, J. Exp. Theor. Phys. **95**, 1044 (2002).